Physica D 241 (2012) 251–259

Contents lists available at SciVerse ScienceDirect

Physica D

journal homepage: www.elsevier.com/locate/physd

Active and passive scalar intermittent statistics in turbulent atmospheric convection

Irene Mazzitelli [a], Alessandra S. Lanotte [b,c,*]

[a] ISAC-CNR Istituto di Scienze dell'Atmosfera e del Clima, Via Fosso del Cavaliere 100, 00133 Roma, Italy

[b] ISAC-CNR Istituto di Scienze dell'Atmosfera e del Clima, Str. Prov. Lecce-Monteroni, 73100 Lecce, Italy

[c] INFN - Sezione di Lecce, 73100 Lecce, Italy

ARTICLE INFO

Article history:
Available online 23 July 2011

Keywords:
Turbulence
Convection
Mixing
Intermittency

ABSTRACT

We study the small-scale statistics of active and passive scalar fields, obtained from 3D large-eddy simulations of the atmospheric boundary layer turbulence. The velocity field is anisotropic and inhomogeneous, due to the action of both buoyancy and shear. We focus on scalar field rare fluctuations dominated by the so-called *fronts*. Temperature, coupled to the velocity field by the Boussinesq equations, exhibits anomalous scaling and saturation of the scaling exponents to a constant value, due to the presence of thermal fronts. Although qualitatively similar, the small-scale statistics of a passive tracer advected by the convective flow shows quantitative differences: the large fluctuations of the tracer concentration field distribute differently and appear to be less intermittent than the temperature ones. To better understand these results, the role of boundaries in this problem is discussed.

1. Introduction

Scalar turbulence is a very broad subject of research, which received a great deal of attention in the past years, particularly in the case of a scalar concentration field passively advected by a turbulent flow [1,2]. This is considered as a prototype of the more complex fully non-linear Navier–Stokes problem, but with the major advantage of being analytically treatable, in some limits (see [3] and the references therein). Here, in particular, we refer to the case of a fully developed turbulent flow (of modest to high Reynolds numbers), passively advecting a scalar field, with Schmidt or Prandtl number order $\sim O(1)$, that is the fluid kinematic viscosity comparable with the scalar molecular diffusivities. For such problems, theoretical, numerical and experimental efforts have successfully led to an understanding of the statistics of the passive scalar provided the following *idealised* conditions are verified: (i) the advecting flow is statistically homogeneous, isotropic and non-intermittent; (ii) the scalar field is statistically homogeneous (not necessarily isotropic) and forced at large scales. Under the previous conditions, scalar increment statistics can be shown to be *universal* with respect to the large-scale forcing and to present *anomalous* or intermittent scaling properties. An important observation is that the scalar signal shows *ramp–cliff* structures (see e.g. [2]), that is regions where scalar fluctuations are weak – cliffs or plateaux – separated by very strong variations across small scale separations, the so-called fronts. These quasi-singular structures play a key role in the scalar statistics: they dominate larger and larger scalar fluctuations, leading to strong small-scale intermittency characterised by the saturation of the scalar moment scaling exponents [4,5].

Note that this is a generic feature: front structures in the trace of passive scalars advected by a turbulent flow are present, regardless of whether the velocity field is two or three dimensional, and regardless of whether large-scale scalar injection is isotropic or not.

Universality and intermittency of passive scalar statistics (within the previous hypothesis) has been understood in terms of Lagrangian interpretation of scalar spatial correlations and statistically preserved structures [3,6,7]. While we cannot review here these results, we note that the same general statements in terms of *universal and anomalous* scaling properties cannot yet be formulated for the problem of active scalar advection.

This is the case of scalar fields which react back on the advecting flow, as e.g. for the atmospheric and Rayleigh–Bénard thermal convection, or for the transport of magnetic fields in two-dimensional conducting flows. The non-linearity, associated with the scalar-flow coupling, rules out the possibility of analytical approaches, while experimental (see e.g. [8]) or numerical [9,10] attempts to gain insight into the problem are not yet conclusive. Clearly, additional difficulties arise if statistical symmetries of turbulent fields, such as isotropy or homogeneity, do not hold or hold only in a weak sense (see [11] for a review on anisotropic

* Corresponding author at: ISAC-CNR Istituto di Scienze dell'Atmosfera e del Clima, Str. Prov. Lecce-Monteroni, 73100 Lecce, Italy. Tel.: +39 06 4993 4289.
E-mail addresses: a.lanotte@isac.cnr.it, alessandra.lanotte@gmail.com (A.S. Lanotte).

0167-2789/$ – see front matter © 2011 Elsevier B.V. All rights reserved.
doi:10.1016/j.physd.2011.07.009

turbulence). A proper theoretical framework for scalar advection in the presence of an intermittent velocity field is also unclear.

So, while at the fundamental level of a theory for active scalar small-scale statistics many questions remain open, at the level of observation it is known that ramp–cliff structures are present also in the trace of active scalars. In the atmospheric temperature field, these are detected in region located from the ground to the middle stratosphere [12]. Hence the question raised is if passive and active scalars have similar statistical behaviours, at least on a phenomenological ground.

In this paper, we study the behaviour of active and passive scalar fields in atmospheric boundary layer (ABL) turbulence, by means of numerical simulations. Transport of scalars is a central problem of atmospherical physics [13], where typically active scalars are the temperature and moisture fields, while passive scalars are gas tracers. The main focus of this work is to characterise scalar small-scale fluctuations, and the role of fronts in the statistics of the temperature and of a gas tracer.

The atmospheric boundary layer convective state is described by means of the Boussinesq approximation for the velocity and temperature fields. In the same flow, a passive scalar is also injected. Since, numerically, we cannot fully describe the range of scales of the 3D atmospheric boundary layer (where typical large scales are $L_0 \simeq 10^3$ m, and the Kolmogorov scale is $\eta \simeq 10^{-3}$ m), we adopt the approach of large-eddy simulations [14]. Within this framework, as specified in the sequel, we can resolve scalar fluctuations over separations larger than tens of metres. Therefore, by small-scale statistics, we intend moments of scalar increments at scales belonging to the inertial range, i.e. over (horizontal) space separations r, such that $0.1 \leq r/z_i \leq 1$, where z_i is the estimated boundary layer height (see below).

The paper is organised as follows. Section 2 describes the model equations and the main features of our numerics; Section 3 contains a characterisation of turbulence for the problem at hand and the main results for the statistics of scalar rare fluctuations. Finally, Section 4 contains the discussion of our results and concluding remarks.

2. Model equations and numerical set-up

Large-eddy simulations (LES) have become a standard tool for numerically studying the atmospheric boundary layer dynamics in the convective regime [15–18], when the energy transfer is dominated by the almost self-similar turbulent energy cascade [19]. In an LES, a low-pass filtering procedure is applied to any turbulent field, thus retaining only the large-scale, most energetic degrees of freedom: (sub-grid) high wavenumber degrees of freedom are parameterised in terms of the low wavenumber ones by statistical closures, such as eddy viscosity or eddy diffusivity closures.

Here, we briefly recall the model equations, the set-up of the numerical simulations, and the main parameters of the runs performed. Filtered or resolved fields are labelled as $\overline{\mathbf{u}}(\mathbf{x}, t)$,

$$\overline{u_i}(\mathbf{x}, t) = \int_{-\infty}^{\infty} \mathrm{e}^{\mathrm{i}\mathbf{k}\cdot\mathbf{x}}\, G(\mathbf{k}, \Delta_f)\, \hat{u}_i(\mathbf{k}, t)\mathrm{d}\mathbf{k},$$

where $G(\mathbf{k}, \Delta_f)$ is the filter function applied in the Fourier space. A sharp spectral filter is applied in the horizontal directions. In the vertical direction, the use of finite differences is equivalent to a top-hat filtering. The LES model advances in time the filtered equations for the temperature $\overline{\theta}(\mathbf{x}, t)$ and the incompressible velocity field $\overline{\mathbf{u}}(\mathbf{x}, t)$, coupled via the Boussinesq approximation [20], and the filtered advection–diffusion equation for the passive concentration field $\overline{c}(\mathbf{x}, t)$. These are:

$$\frac{\partial \overline{u}_i}{\partial t} = -\frac{\partial \overline{\overline{u}_i}\overline{u}_j}{\partial x_j} - \frac{\partial P^\star}{\partial x_i} + g\frac{\overline{\theta}}{\theta_0}\delta_{iz} + f_c\epsilon_{ijz}(\overline{u}_j - U_{gj}) - \frac{\partial \tau_{ij}^d}{x_j}, \tag{1}$$

$$\frac{\partial \overline{u}_i}{\partial x_i} = 0, \tag{2}$$

$$\frac{\partial \overline{\theta}}{\partial t} = -\frac{\partial \overline{\overline{u}_i}\overline{\theta}}{\partial x_i} - \frac{\partial \tau_i^{(\theta)}}{\partial x_i}, \tag{3}$$

$$\frac{\partial \overline{c}}{\partial t} = -\frac{\partial \overline{\overline{u}_i}\overline{c}}{\partial x_i} - \frac{\partial \tau_i^{(c)}}{\partial x_i}. \tag{4}$$

Here the indexes i, j are running over x, y, z ($u_x = u$, streamwise, $u_y = v$, spanwise, $u_z = w$, wall-normal component), and repeated indexes are retained summed. In the above equations, g is the acceleration due to gravity directed along z, θ_0 is a reference temperature, f_c is the Coriolis parameter. U_{gj} is the j component of the external geostrophic wind, which balances the mean horizontal pressure gradient; τ_{ij}^d is the deviatoric part of the residual (or subgrid scale SGS) strain tensor τ_{ij}, which is defined according to

$$\tau_{ij} = \overline{u_i u_j} - \overline{u}_i\overline{u}_j = \overline{\overline{u}_i u_j'} + \overline{u_i'\overline{u}_j} + \overline{u_i' u_j'}, \tag{5}$$

where the vector components u_i' are the unresolved parts of the turbulent field: $u_i(\mathbf{x}, t) = \overline{u}_i(\mathbf{x}, t) + u'(\mathbf{x}, t)$.

The isotropic component of the strain (5) is included in the pressure term:

$$P^\star = \frac{\overline{p}}{\rho_0} + \frac{\tau_{kk}}{3} + \frac{(\overline{\overline{u}_k}\overline{u}_k)}{2},$$

with $\bar{p}$ the physical pressure and ρ_0 the air density. In the scalar equation, the SGS stress for the temperature θ or equivalently for the tracer c has the form:

$$\tau_i^{(\theta)} = \overline{\theta\, u_i} - \overline{\theta}\overline{u}_i = \overline{\overline{\theta} u_j'} + \overline{\theta'\overline{u_i}} + \overline{\theta' u_i'}. \tag{6}$$

We have modified the numerical code, developed at the National Center for Atmospheric Research (NCAR) [21], by replacing the Smagorinsky closure for the stress terms in Eqs. (5) and (6) with the so-called Dynamic Model [22,23].

Standard 2/3-idealised pseudo-spectral space integration is performed in the horizontal directions, while a finite-difference second-order scheme is adopted for space integration along the vertical direction. Time evolution is implemented by a Runge–Kutta third order scheme.

The 3D physical domain, with spatial dimensions $L_x \times L_y \times L_z$, is homogeneous in the horizontal planes; along the vertical direction, there is a wall at the bottom and an open surface at the top. In the present study, $L_x = 5000$ m, $L_y = 5000$ m, and $L_z = 2000$ m. We performed two numerical experiments with 256^3 collocation points, hence the mesh spacing is about 20 m × 20 m × 8 m. The values of the relevant parameters for the numerical simulations are collected in Table 1. Note that the typical integral scale in the horizontal directions is about $L_0 \simeq 1.5\, z_i$ [24], where z_i is the atmospheric boundary layer height which fixes the vertical integral scale.

Velocity field fluctuations are generated by both buoyancy and shear. The velocity field satisfies a no-sleep condition at the bottom wall, while it matches the large-scale geostrophic wind at the free top. Temperature fluctuations are generated via a constant in time, homogeneous in space, surface heat flux H_0 mimicking the response of the ground to solar radiation: here $H_0 = \langle(\overline{w} - \langle\overline{w}\rangle)(\overline{\theta} - \langle\overline{\theta}\rangle)\rangle$, and the average is performed on the horizontal planes close to the surface. The close-to-the-wall region where the heat flux does not vary with height is known as *surface layer*.

As a result of the surface heating and the mechanical stirring by shear, a quasi-steady state is reached for the velocity and temperature fields. Concentration fluctuations are also generated by a constant in time, homogeneous in space, surface concentration flux C_0, which guarantees a quasi-steady state for the passive tracer

Table 1
Internal parameters. Run S (W) presents a strong (weak) initial temperature gradient (capping inversion) Γ_0 at the top of the boundary layer. Other symbols in the table: z_i is the boundary layer height (estimated as the height of minimum vertical heat flux); w_* is the typical vertical velocity value or convective velocity scale, $w_* = (gz_iH_0/\theta_0)^{1/3}$; $\tau_* = z_i/w_*$ is the large-scale eddy turn-over time; $-z_i/L$, where L is the Monin–Obukhov length [24], is the stability parameter indicating for our runs a moderate convective regime; $|\Delta c|$ is the initial tracer concentration jump across the entrainment zone at the top layer; C_0 is the passive tracer surface flux, and C_{in} is the estimated initial passive tracer entrainment flux; Γ_0 is the temperature gradient across the entrainment layer; H_0 is the surface heat flux, and H_{in} is the estimated initial entrainment heat flux.

Run	z_i (m)	w_* (m s^{-1})	τ_* (s)	$-z_i/L$	$\lvert\Delta c\rvert$ (ppm)	C_0 (ppm m s^{-1})	C_{in} (ppm m s^{-1})	Γ_0 (K m^{-1})	H_0 (K m s^{-1})	H_{in} (K m s^{-1})
S	1080	2.1	520	23	0.1	0.2	0.006	0.1	0.24	−0.04
W	1400	2.3	610	27	10	0.2	0.3	0.01	0.24	−0.04

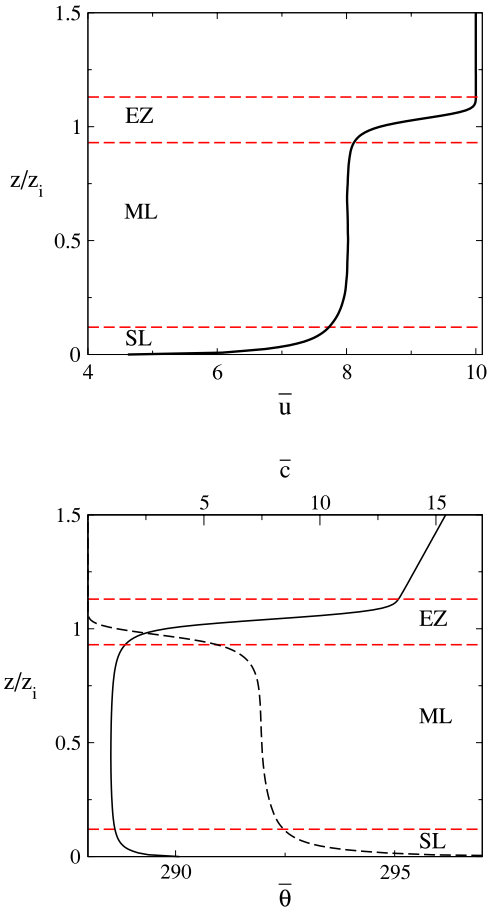

Fig. 1. Vertical mean profiles of the turbulent fields as functions of z/z_i, where z_i is the atmospheric boundary layer height. (Top) streamwise component of the velocity field $\bar{u}$ ((m/s) units), approaching the imposed geostrophic wind $U_g = 10$ m/s at the top of the domain. (Bottom) the scalar temperature $\bar{\theta}$ (Kelvin degree units) is indicated by a continuous line, while the scalar concentration $\bar{c}$ profile (ppm units) is the dashed line. In the figures, it is made the distinction among the surface layer (SF), the mixed layer (ML) and the entrainment zone (EZ).

field. Because of the action of turbulent convection, temperature and concentration mean vertical profiles are constant with height in the physical domain, not too close to the boundaries: the region where this happens is known as the *mixed layer* [24]. In Fig. 1, typical vertical profiles of the mean velocity, temperature and concentration fields are shown.

Near the top of the domain, the temperature field matches an imposed positive mean gradient, whose magnitude can be varied, mimicking the stably stratified layer of free atmosphere capping the atmospheric boundary layer. That region of matching is called *entrainment layer*.

The scalar concentration is set to zero in the free atmosphere, where no scalar sources are generally expected. Initial conditions are assigned according to standard profiles of velocity, temperature and concentration fields in the ABL; we simulated two different conditions: case S, where the top temperature gradient Γ_0 is strong and the initial concentration jump across the entrainment layer $|\Delta c|$ is small; case W, where the top temperature gradient is weak and the initial concentration jump across the entrainment layer is large. As a result, different concentration entrainment fluxes C_{in} establish at the top of the mixed layer.

The atmospheric boundary layer quasi-steady state is characterised by stationary momentum mean vertical profile, and by scalars mean vertical profiles which can change in time (for example the mean temperature in the mixed layer grows, as it generally happens in the atmospheric boundary layer during diurnal convection). Total variances are statistically stationary for all turbulent fields, except in run S, where the passive tracer variance shows a slowly growing trend.

The integration is carried out for about thirty large-scale eddy turn-over times τ_*, after the transient stage lasting few eddy turn-over times was finished. To limit the effects associated with deviations from steadiness in run S, we performed the statistical analysis over $\simeq 20\tau_*$, by saving 80 snapshots equally spaced in time. Within this interval, the above mentioned variance growth is small.

The mixed layer is characterised by almost constant profiles of the kinetic energy turbulent dissipation, and scalar fluctuation dissipations. In the surface layer, dissipations are maximal because of the local strong gradients. Turbulent dissipations rapidly decrease to zero in the viscous sub-layer, close to the wall, not resolved in our LES, where all turbulent fields have an almost linear mean profile [24]. In the entrainment layer, dissipation rates decrease to zero also, since in the stably-stratified free atmosphere there is neither mechanical nor thermal production of turbulence.

In our numerics, eddy diffusivities of the temperature and passive tracer fields are almost equal, but larger than the momentum eddy viscosity: the SGS Prandtl and Schmidt numbers evaluated in terms of eddy-dissipation coefficients turn out to be $\simeq 0.35$. In an LES, Reynolds number estimation is rather uncertain, but, in our range of parameters, Taylor scale based Reynolds number is of the order of a few thousands.

We notice that the top of the boundary layer *injects* positive temperature fluctuations (acting as a temperature source), and negative concentration fluctuations (acting as a passive tracer sink). For the temperature field, the magnitude of the positive entrainment flux is always smaller than the bottom one. Warm thermal plumes are generated near the bottom surface, then rise and broaden in the mixed layer; wider but *weaker* and colder plumes descend from the top of the boundary layer towards the bottom surface. For the passive concentration field, the relative magnitude of the entrainment and the bottom fluxes depend on the imposed boundary conditions. If the concentration surface flux C_0 is much larger than the entrainment one C_{in}, the passive tracer behaviour is driven by the bottom surface in almost the entire mixed layer. Passive tracer fluctuations tend to strongly correlate with the temperature field, and the passive tracer field is *trapped* into the rising thermal plumes. On the other hand, if concentration surface flux is much smaller than the top one, passive scalar mixes *independently* of the temperature field.

Both scalar fields distribute in regions of nearly constant value, separated by thin layers of sharp scalar gradients; however, when

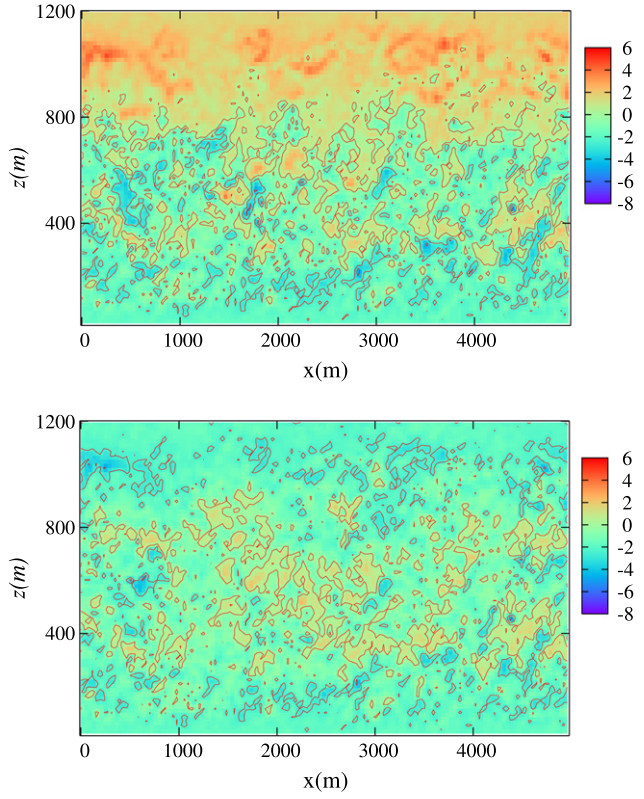

Fig. 2. Skewness of temperature (top) and concentration (bottom) vertical gradients, averaged along the spanwise direction y, as function of x and z. Data refer to a snapshot of the scalar fields within run S. The instantaneous boundary layer height is $z_i \simeq 940$ m. Contour lines are plotted on levels -5, -2.5 and 0.

$C_{in}/C_0 > 1$, regions of homogeneous tracer concentration and regions of tracer sharp gradients (fronts) are on average spatially uncorrelated with those of the temperature field. If the ratio C_{in}/C_0 is neither too small nor too strong, the statistical correlation of the scalars depends on the height z in the mixed layer, making the system inherently inhomogeneous.

Fig. 2 shows the skewness of vertical scalar derivative,

$$\mathcal{S} = \langle(\partial_z\bar{\theta})^3\rangle/\langle(\partial_z\bar{\theta})^2\rangle^{3/2},$$

averaged along the spanwise direction y, evaluated on snapshots of the temperature and of the concentration fields, for run S. The (light blue) dark shade, near the surface, reveals the positive fluxes of both temperature and concentration from the surface. Similar structures for the temperature and concentration skewness in the lower layer signal a strong spatial correlation at small scales between the two scalar fields. On the other hand, opposite processes are occurring at the top of the mixed layer. There, positive temperature fluctuations are associated to the entrainment of warm air, whereas negative concentration fluctuations are associated to the entrainment of clean air parcels.

In each numerical simulation, the statistical measurements were carried out in a limited vertical region, where turbulent fields are almost isotropic in the horizontal (homogeneous) planes and with vertical inhomogeneity effects smaller than the statistical error bars. In this region, variances of turbulent scalar fields do not vary with height. In the sequel, unless specified, the measurements shown are performed in the horizontal planes, and averaged along the vertical direction for planes belonging to the selected region: $0.4 < z/z_i < 0.6$. We remark that in this selected region, the two series of numerical experiments, run W and run S, exhibit the same small-scale statistical behaviours, within error bars. Hence, we expect to have a reduced dependence on the boundary conditions on the statistical analysis performed.

Finally, note that LES models have been used to study resolved scales turbulent fluctuations in many different contexts; see e.g. [25,26]. Results have been shown to be independent of the LES model adopted and robust with respect to the spatial resolution.

3. Temperature and concentration statistics

Classical theory for thermal convection (see e.g. [27]) predicts the scaling behaviour of the turbulent velocity and temperature fields, balancing buoyancy forces and inertial ones. The Bolgiano length L_B defines the scale at which these forces are comparable. At scales larger than L_B, yet smaller than the large-scale correlation length L_0, kinetic energy transfer should be dominated by buoyancy forces, leading to the Bolgiano–Obukhov (BO) scaling for the velocity and temperature increments, namely for $L_B \ll r \ll L_0$, $\langle\{[\mathbf{u}(\mathbf{x}+\mathbf{r})-\mathbf{u}(\mathbf{x})]\cdot\hat{\mathbf{r}}\}\rangle \propto (r/L_0)^{3p/5}$ and $\langle[\theta(\mathbf{x}+\mathbf{r},t)-\theta(\mathbf{x},t)]^p\rangle \propto (r/L_0)^{p/5}$. Moreover, by dimensional argument, the same scaling properties of the temperature field should apply to the passive scalar $\bar{c}$.

Differently, for scales $\eta \ll r \ll L_B$, where η is the Kolmogorov scale of the flow, inertial forces should dominate, imposing a constant rate of kinetic energy transfer towards the small scales, i.e. the Kolmogorov–Obukhov–Corrsin (KOC) scaling: $\langle\{[\mathbf{u}(\mathbf{x}+\mathbf{r})-\mathbf{u}(\mathbf{x})]\cdot\hat{\mathbf{r}}\}\rangle \propto (r/L_0)^{p/3}$ and $\langle[\theta(\mathbf{x}+\mathbf{r},t)-\theta(\mathbf{x},t)]^p\rangle \propto (r/L_0)^{p/3}$. Let us emphasise that, being a dimensional argument, the inertial Bolgiano–Obukhov scenario does not take into account neither the role of boundaries, nor the direction of the kinetic energy cascade. Bolgiano–Obukhov scenario (corrected by intermittency for the temperature field) has been clearly observed in 2D turbulence [28], where however the velocity fluctuations are not intermittent and kinetic energy cascades from the small to the large scales of the flow. In 3D turbulence, where kinetic energy cascade goes from large to small scales (direct cascade), the results are not yet conclusive [29].

Experiments in a Rayleigh–Bénard cell, where also a fluorescent dye is injected [8], give indications of different scaling properties between active and passive scalars, above and below the Bolgiano scale. Indications of the simultaneous presence of both the BO and KOC behaviours have been reported in direct numerical simulations of a Rayleigh–Bénard convective cell [30], where however the limited range of scales does not allow for conclusive statement. What emerges is that the interaction of the velocity field with the wall is important to obtain a Bolgiano length smaller than the integral scale of the flow.

In Fig. 3, we report two measurements of the Bolgiano scale L_B obtained in our numerics. Classical definition of L_B is the length at which inertia balances buoyancy forces, resulting in

$$L_B = \frac{\epsilon^{5/4}}{N^{3/4}(g/\theta_0)^{3/2}}. \tag{7}$$

In our set-up, the kinetic energy dissipation rate ϵ and the scalar thermal dissipation rate N are averaged on the horizontal planes since they both vary along the vertical axis.

More recently, it has been proposed [30,31] to define L_B as the scale at which energy transfer by inertial effects is comparable with that associated to buoyancy, giving,

$$\epsilon(z) \simeq (g/\theta_0)\langle|\delta w(r=L_B)\,\delta\theta(r=L_B)|\rangle, \tag{8}$$

with averages performed over the horizontal planes. Both definitions are dimensional and thus valid up to a non-dimensional prefactor that we cannot control: if we allow for an arbitrary constant $\sim O(1)$, the two estimations coincide. In Fig. 3, Bolgiano lengths are normalised with the size of the physical domain in the horizontal directions. In the entire domain, buoyancy seems to be the dominant mechanism for the energy transfer; however we do not expect to have enough range of scales to see

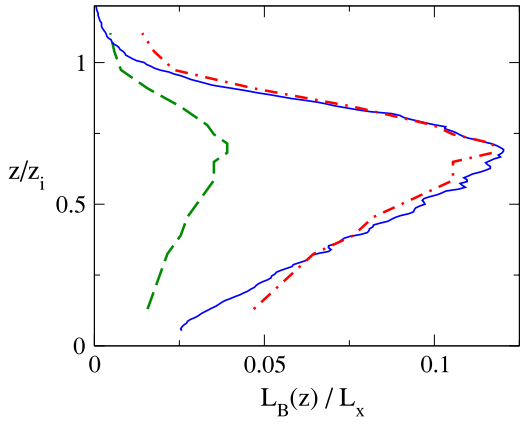

Fig. 3. (Green dashed curve) Vertical profile of the Bolgiano scale obtained from Eq. (8), normalised with the horizontal size of the domain; (blue continuous curve) the Bolgiano scale obtained from Eq. (7); (red dot-dashed curve) L_B from Eq. (8) multiplied by a prefactor $C = 3$. Same prefactor is found in the Rayleigh–Bénard DNS [30].

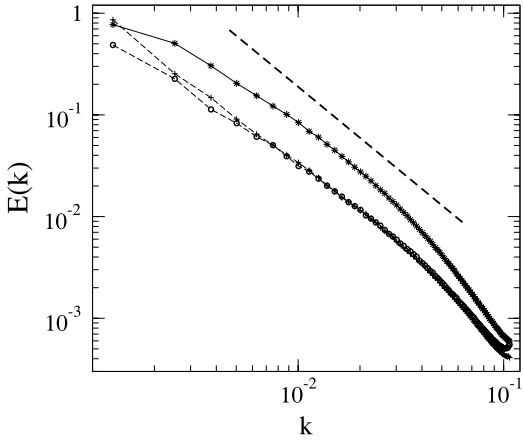

Fig. 4. Log–log plot of the one dimensional turbulent spectra measured along the streamwise direction for run W. Symbols: (Stars) for the streamwise velocity component $\bar{u}$, (plus) for the temperature $\bar{\theta}$, (circles) for the concentration $\bar{c}$. The dashed curve has a slope $\simeq k^{-5/3}$. Average is performed over the horizontal planes with $0.45 < z/z_i < 0.6$.

the BO scaling. Indeed, in the region where we perform our measurements, the Bolgiano length is only a factor five smaller than the horizontal integral scale $L_0 \simeq 2100$ m. The absence of BO scaling is confirmed by the inspection of the 1D spectra measured along the streamwise direction, shown in Fig. 4. Turbulent spectra for velocity, temperature and tracer fields are compatible with a Kolmogorov scaling $E(k) \simeq k^{-5/3}$ [32]. Notice that, at a low order such as the second statistical moment, the two scalars exhibit an equal behaviour at any spatial scale except the large ones.

Before focusing on small-scale features, it is useful to look at the scalar distributions. In [33], the behaviour of the probability density functions (PDFs) $P(\bar{\theta} - \langle\bar{\theta}\rangle)$, $P(\bar{c} - \langle\bar{c}\rangle)$ (average is on the horizontal planes) is discussed, at varying the injection mechanism (run S *vs.* run W), and the distance from the bottom surface. Due to the imposed boundary conditions, the temperature field is not very sensitive to these variations, while the concentration field can display important differences in the large scale features. In particular, as shown in Fig. 5, the temperature single-point PDF is always strongly positively skewed, while the concentration one can be differently negatively skewed.

What are the consequences of these different large-scale features on the small-scale statistics? Are the presence of fronts and their statistical role universal, i.e. independent of the large

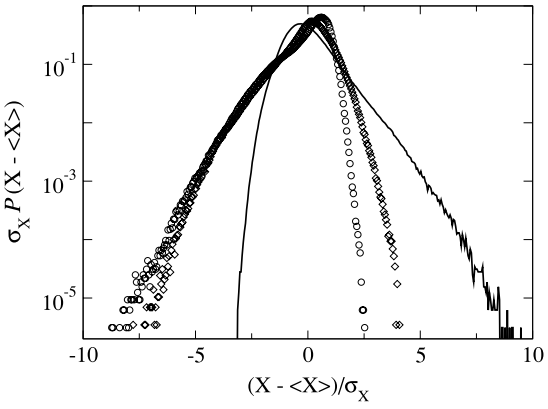

Fig. 5. Lin–log plot of the single point probability density function $P(X - \langle X\rangle)$, where X is either the resolved temperature $\bar{\theta}$ or the resolved concentration $\bar{c}$. PDFs are measured at $z/z_i = 0.65$ and averaged over all available statistics. The continuous line is for the temperature field in run W (same curve is obtained in run S, not shown). Diamonds are for the PDF of the tracer field in run S, while open circles are for the tracer field in run W.

scales of turbulence? Or do they change at varying top/bottom fluxes? In the sequel, we try to answer these questions.

3.1. Saturation of intermittency of scalars

A way to characterise scalar fluctuations is in terms of the so-called structure functions,

$$S_p(r) \equiv \left\langle [\bar{c}(\mathbf{x}+\mathbf{r},t) - \bar{c}(\mathbf{x},t)]^p \right\rangle = \langle (\delta_{\mathbf{r}}\bar{c})^p \rangle \propto (r/L_0)^{\xi_p} ,$$

where we have assumed that the scalar field is stationary, statistically homogeneous and isotropic. If the statistical ensemble is anisotropic but homogeneous, these moments do not depend on the point of measure ($\mathbf{x}$), but possibly only of the direction of the separation vector ($\mathbf{r}$).

The Kolmogorov–Obukhov–Corrsin (KOC) theory predicts for even order structure functions of passive scalar fields a dimensional (non-intermittent) behaviour

$$S_{2p}(r) = C_{2p} N_c^p \epsilon^{-p/3} r^{2p/3} \propto (r/L_0)^{\xi_p} , \tag{9}$$

where C_{2p} are non-dimensional constants, N_c is the tracer dissipation rate, and the scaling exponents linearly increase with the moment order p, $\xi_{2p} = 2p/3$.

An important result of experimental and numerical research over the past fifteen years has been confirming that, as predicted by recent theoretical models (see [3] for a review), passive scalar fields display an extremely intermittent statistics, leading to saturation of the scaling exponents: i.e., given $\langle [c(\mathbf{x}+\mathbf{r},t) - c(\mathbf{x},t)]^p \rangle \simeq (r/L_0)^{\xi_p}$, the exponents ξ_p tend to a constant value $\xi_p \to \xi_\infty = const.$, for large enough orders $p > p_{crit}$ [5,34],

$$S_p(r) = \left\langle (\delta_r \bar{c})^p \right\rangle \propto (r/L_0)^{\xi_\infty} , \quad p > p_{crit} .$$

Here, the exponent $\xi_\infty > 0$ has to be positive [35] and no longer depends on the order p. This is the largest possible deviation from the dimensional linear scaling of the KOC theory. According to the KOC theory, moments of order $2p$ are simply the square of moments of order p, while when saturation is observed, if $p > p_{crit}$ all moments scale with the same exponent ξ_∞.

Saturation of structure function exponents is the statistical counterpart of the presence of fronts in the scalar fields [5]. To explain this, we start by giving an operative definition of scalar front. We call front a scalar excursion whose amplitude stays of the order of few standard deviations, with the minimal thickness r that can shrink down to be of the order of the Kolmogorov dissipative scale (that we do not resolve here):

$$\delta_r \bar{c} > \lambda \sigma_{\bar{c}} ,$$

where λ is a positive constant $\lambda > 1$, and the separation r is taken in the inertial range of scales $\eta < r < L_0$. Clearly, to measure larger excursions, larger statistical datasets are needed.

From the previous description, it is clear that nearby locations can exhibit very large differences of scalar concentration, and these quasi-singularities dominate the behaviour of extreme events (partly resembling what happens in Burgers turbulence because of shocks in the velocity field [32]). Note that in 2D and 3D turbulence, passive scalar statistics converge more slowly than velocity statistics, hence wide scale separation and large statistical samples are required to obtain accurate and reliable data [36].

In the case of active scalars, saturation of scaling exponents of the temperature field, $\langle[\theta(\mathbf{x}+\mathbf{r},t)-\theta(\mathbf{x},t)]^p\rangle \propto (r/L_0)^{\zeta_\infty}$ for large p, has been observed in 2D direct numerical simulations of homogeneous thermal convection [28] (i.e. without boundaries), and in 3D experiments in a Rayleigh–Bénard cell [37]. Saturation of temperature intermittency has also been measured in a numerical study of the atmospheric boundary layer convection by means of large-eddy simulations [25].

Coming to the investigated ABL, a striking feature is that in both runs W and S, scalar increment distributions $P(\delta_r\bar{\theta})$ and $P(\delta_r\bar{c})$, at separations r in the inertial range, strongly deviate from a Gaussian curve and exhibit large deviations from mean values. For a quantitative analysis, it is natural to consider either the behaviour of high-order structure functions or, equivalently, the scaling of the very broad tails of scalar increment PDFs [5,38]. We adopted the latter procedure, which is less affected by finite size effects. Saturation implies that the probability density function of scalar increments has the following form [38]

$$\mathcal{P}(\delta_r\bar{c}) = \frac{r^{\xi_\infty}}{\sigma_{\bar{c}}}\,\mathcal{G}\left(\frac{\delta_r\bar{c}}{\sigma_{\bar{c}}}\right), \tag{10}$$

$$\mathcal{P}(\delta_r\bar{\theta}) = \frac{r^{\zeta_\infty}}{\sigma_{\bar{\theta}}}\,\mathcal{Q}\left(\frac{\delta_r\bar{\theta}}{\sigma_{\bar{\theta}}}\right), \tag{11}$$

for increments $\delta_r\bar{c} > \lambda\sigma_{\bar{c}}$ larger than the scalar standard deviation $\sigma_{\bar{c}} = \langle(\bar{c}-\langle\bar{c}\rangle)^2\rangle^{1/2}$, and equivalently for the temperature fluctuations. The power-law form for the tails of the scalar increment PDFs means that large scalar differences are dominated by the same statistical objects, and the probability to have a fluctuation, which is order $\sigma_{\bar{c}}$ across a distance r, goes as r^{ξ_∞}.

In these expressions, the unknown functions $\mathcal{Q}(\cdot)$ and $\mathcal{G}(\cdot)$ do not depend on the scale separation r and are bounded by the single point scalar distribution [38].

The functional shapes in Eqs. (10) and (11) determine the behaviours of structure functions. From the definition:

$$S_p(r) = \int_{-\infty}^{\infty}(\delta_{\mathbf{r}}\bar{\theta})^p\,\mathcal{P}(\delta_{\mathbf{r}}\bar{\theta})\mathrm{d}(\delta_{\mathbf{r}}\bar{\theta}), \tag{12}$$

if we insert expression (11), valid for large scalar excursion or high order moments (i.e. large p), we obtain

$$\begin{aligned} S_p(r) &= \sigma_{\bar{\theta}}^p\, r^{\zeta_\infty}\int_{-\infty}^{\infty}\frac{\delta_r\bar{\theta}^p}{\sigma_{\bar{\theta}}^p}\mathcal{Q}\left(\frac{\delta_r\bar{\theta}}{\sigma_{\bar{\theta}}}\right)\mathrm{d}\left(\frac{\delta_r\bar{\theta}}{\sigma_{\bar{\theta}}}\right) \\ &= A_p\sigma_{\bar{\theta}}^p\, r^{\zeta_\infty}. \end{aligned} \tag{13}$$

Integral on the right hand side of the previous expression is finite, since the function $\mathcal{Q}\left(\frac{\delta_r\bar{\theta}}{\sigma_{\bar{\theta}}}\right)$ is bounded on the very far tails [38].

A geometrical interpretation of the saturation exponent ξ_∞ or ζ_∞ is natural [32]. If we define D_F the fractal (non-integer) dimension of the set hosting scalar fronts, then $D_F = d-\xi_\infty$, where d is the space dimension where fronts are measured. Since in our analysis we measured scalar increments in horizontal planes, then $d = 2$.

Note that, in general 3D flows, there is no strong argument to expect equal statistics and thus equal saturation exponents for the two scalars, i.e., $\xi_p = \zeta_p$ for any order p. Indeed, equal and universal statistics for active and passive scalar fields has been proven only for 2D thermal convection in the presence of an inverse energy cascade for the velocity field (which is non intermittent) [28], or in the case of a shell-model for the same problem (again in the presence of a non-intermittent velocity field) [39].

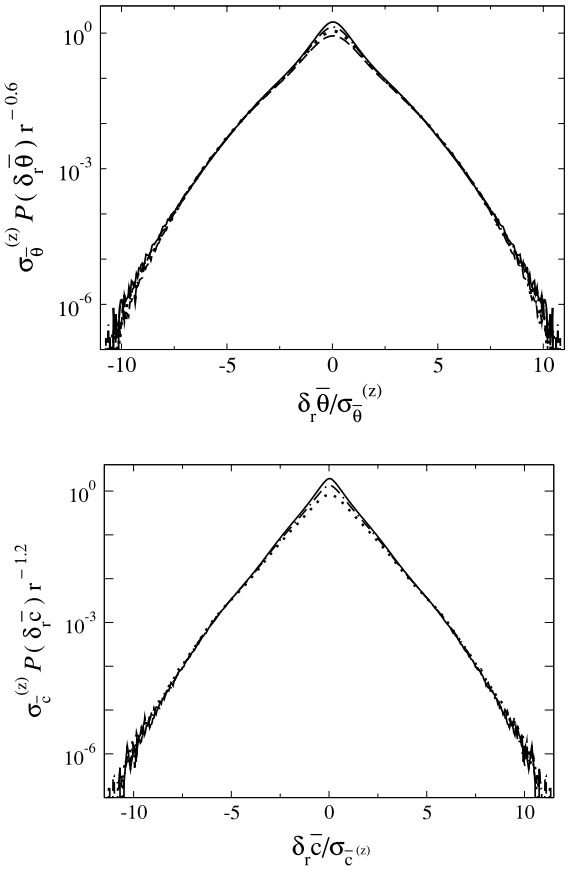

Fig. 6. (Top) Lin–log plot of the temperature increments probability density function, multiplied by the factor $\sigma_{\bar{\theta}}(z)/r^{\zeta_\infty}$. They are taken at four different scale separations $r/z_i \simeq 0.26$ (solid line), 0.36 (dot-dashed line), 0.45 (dotted line), and 0.59 (dashed line). The z-dependent temperature standard deviation $\sigma_{\bar{\theta}}(z)$ used to normalise the PDFs is the one corresponding to the average over the horizontal planes with $0.45 < z/z_i < 0.6$. (Bottom) The same for the concentration field, at the scales $r/z_i \simeq 0.36$ (solid line), 0.45 (dot-dashed line) and 0.59 (dotted line).

Let us move to the results obtained in our numerical simulations. In Fig. 6 (top), we show the PDFs $\mathcal{P}(\delta_r\bar{\theta})$ of scalar increments for different values of the scale r inside the inertial range of scales, multiplied by the factor $\sigma_{\bar{\theta}}/r^{\zeta_\infty}$. Temperature increments are measured along the spanwise direction y, to reduce anisotropic effects due to the thermal plumes and shear. The collapse of the tails of the probability density functions indicates the presence of saturation, since they all scale as power-laws with the same saturation exponent, and also gives the unknown function $\mathcal{Q}\left(\delta_r\bar{\theta}/\sigma_{\bar{\theta}}\right)$ in Eq. (11).

The saturation exponent measured for the temperature field $\zeta_\infty = (0.6\pm0.2)$ coincides with the result already obtained in [25], in a similar set-up for the atmospheric boundary layer convection. In the same figure, (bottom) we plot the PDFs $\mathcal{P}(\delta_r\bar{c})$ for the tracer field, at the same values of the scale r, multiplied by the factor $\sigma_{\bar{c}}/r^{\xi_\infty}$, with $\xi_\infty = (1.2 \pm 0.2)$. These plots refer to run W but similar results have been obtained in run S.

Another way to probe the role of fronts in the scalar statistics is by considering the cumulative probability of measuring large fluctuations. By integrating equation (11), one obtains that the cumulative probability of large fluctuations (larger than $\lambda\sigma_{\bar{\theta}}$)

$$\mathcal{P}(|\delta_r\bar{\theta}| > \lambda\sigma_{\bar{\theta}}) = \int_{-\infty}^{-\lambda\sigma_{\bar{\theta}}}\mathcal{P}(\delta_r\bar{\theta})\mathrm{d}(\delta_r\bar{\theta}) + \int_{\lambda\sigma_{\bar{\theta}}}^{\infty}\mathcal{P}(\delta_r\bar{\theta})\mathrm{d}(\delta_r\bar{\theta}), \tag{14}$$

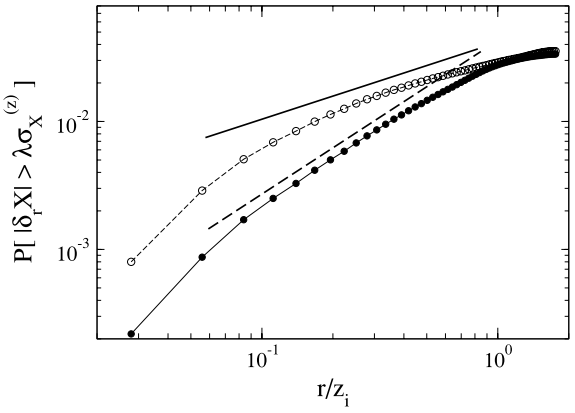

Fig. 7. Log–log plot of the cumulative probability density function of scalar increments larger than $\lambda\sigma_X(z)$, with $\lambda = 3.5$: (empty circles) for the temperature, and (filled circles) for the concentration. Scalar increments are measured along the spanwise direction y. The z-dependent standard deviation $\sigma_X(z)$ used to compute cumulative PDFs is the one corresponding to the average over the horizontal planes with $0.45 < z/z_i < 0.6$. The straight lines have the following slopes: $\simeq r^{0.6}$ (solid line), $\simeq r^{1.2}$ (dashed line).

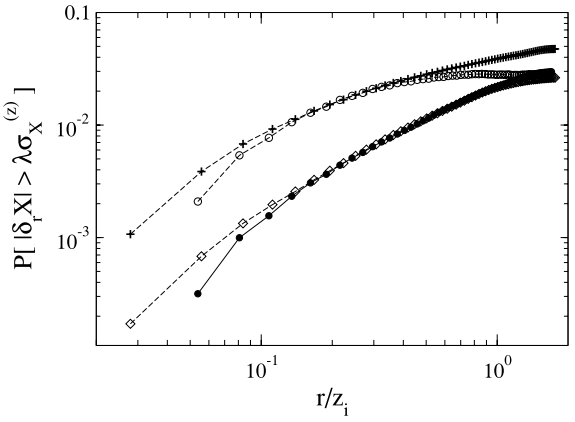

Fig. 8. Log–log plot of the cumulative probability density function of scalar increments larger than $\lambda\sigma_X(z)$, with $\lambda = 3.5$: (empty circles) for the temperature, and (filled circles) for the concentration in run $W128$ with 128^3 grid points. Scalar increments are measured along the spanwise direction y. The z-dependent standard deviation $\sigma_X(z)$ used to compute cumulative PDFs is the one corresponding to the average over the horizontal planes with $0.15 < z/z_i < 0.3$. Data from run W with 256^3 grid points are also plotted. These are the same data of the previous figure, here shifted vertically by an arbitrary factor to superpose the curves. (Plus symbols) for the temperature, and (empty diamonds) for the concentration.

behaves as $\mathcal{P}(|\delta_r\bar{\theta}| > \lambda\sigma_{\bar{\theta}}) \propto r^{\zeta_\infty}$, if we choose the constant λ greater than one. In Fig. 7, the scaling behaviour of the scalar cumulative probability density functions obtained in run W is plotted for $\lambda = 3.5$. Here the differences of large fluctuation statistics for the temperature and the concentration fields are even more manifest.

We are not aware of previous measurement of passive scalar saturation exponent in 3D convective flows. Indeed, for 3D flows, the scalar saturation exponent has been measured only in the case of homogeneous and isotropic turbulence in liquid helium [34], where authors report the value $\xi_\infty^{iso} = (1.4 \pm 0.1)$. The two measurements are compatible. However in the present system the velocity field, whose spectrum is also Kolmogorov like, is more complex due to convection and anisotropy, so discrepancies might well arise [40]. We remark that similar figures are obtained for other values of the constant $\lambda \in (1; 4.5]$ (not shown).

To summarise, we have measured the statistics of large fluctuations of the two scalar fields, in a region of the convective boundary layer where inhomogeneity effects are very small. The two fields are driven by the same velocity field. Both exhibit strong intermittency with saturation of structure function scaling exponents, or equivalently power-law behaviour for the scalar increment PDF tails, due to the presence of quasi-singular structures in the trace of the scalar fields. However, the saturation scaling exponents are different, implying that the fronts have different geometrical features.

Run W and run S produce similar results, which point to the universality of the scalar statistics with respect to the large-scale conditions. Next we further investigate scalar turbulence universality, by reporting results from another series of numerical simulations.

3.2. The role of boundaries

In run W and S, temperature and concentration fields present entrainment fluxes of different signs (see Table 1). Indeed, due to the applied positive temperature gradient Γ_0, the top boundary behaves as a source for the temperature field. Conversely, due to the negative tracer gradient, the top boundary is a sink for the concentration (see Section 3 and discussion therein).

In the present section, we focus on the possible role of different boundary conditions on the statistics of the two scalars well inside the mixed layer. In particular, we want to check whether previous results are universal or not with respect to the large-scale fluxes, imposed at the boundaries. We performed a simulation with the same physical domain but at lower resolution, with 128^3 grid points: the initial temperature inversion is $\Gamma_0 = 0.08$ K/m and the temperature fluctuations are convectively driven by the homogeneous, constant in time surface flux $H_0 = 0.24$ K m/s (run $W128$). In this simulation the concentration field is forced to match a *positive* top gradient, which results in a negative entrainment flux $C_{in} \simeq -0.01$ ppm m/s. The concentration homogeneous surface forcing is perturbed in time with random fluctuations around the mean value $C_0 \simeq 0.05C_{in}$. Random fluctuations are added to break spatial correlations among scalars near the bottom. Therefore, though quantitatively different, similar constraints are applied to both temperature and concentration on the top and on the bottom surfaces, except for the randomisation at the surface. Owing to the large C_{in}/C_0 ratio, a wide vertical region is created where concentration fluctuations are sufficiently decorrelated from temperature ones. In such regions, extending in the range $0.15 < z/z_i < 0.3$, the linear correlation coefficient, averaged in the horizontal planes, between θ and c is close to zero.

We investigate the high order scalar statistics in this mixing region. In Fig. 8, we compare the cumulative probability of large temperature/concentration fluctuations, evaluated in run $W128$, with results of run W at larger resolution. The agreement is rather good, especially for concentration increments. The discrepancy that occurs between temperature values at large scales is due to the different location of the vertical regions selected in the two simulations to perform the statistical analysis.

Thus we conclude that the difference in active and passive scalar behaviour discussed in the previous section cannot be attributed to qualitatively different fluxes through the entrainment zone. Two remarks are in order. First, the obtained results are robust with respect to change of the spatial resolution and of the large scale conditions. This implies that cumulative PDFs behaviour is universal in the scaling laws (power-law exponents ζ_∞ do coincide), but not in the prefactors (the two curves are shifted in amplitude).

Second, the different scaling behaviours of the two scalars do not depend on the way scalar fluctuations are produced, provided scalar injection is realised via statistically independent realisations. In this particular set-up, such a condition is obtained by modulating the relative magnitude of the entrainment concentration flux with respect to the surface flux. This factor plays a key role in breaking large-scale spatial correlation between temperature and concentration.

4. Conclusions

Turbulent convection is characterised by the presence of plumes, whose edges are often the location of strong temperature gradients. However, as we have discussed, front structures seem to be a general feature of scalar spatial organisation. Small-scale spatial structures are also vorticity filaments in incompressible Navier–Stokes turbulence or vortex sheets in magnetohydrodynamical turbulence, but their statistical signature is not as strong as in the case of scalar turbulence: indeed, in none of these cases, saturation of intermittency is observed.

In this work, we have numerically studied the statistics of an active and of a passive scalar field, driven by the same turbulent flow, generated by the atmospheric boundary layer convection. The present set-up is complex since the system is neither fully homogeneous, nor isotropic. Moreover, small-scale statistics is measured on large-eddy simulation fields, which makes more difficult to obtain very clean datasets. Within these limitations, we have collected large statistical samples and performed an accurate analysis of the effects due to the choice of different boundary conditions. Indeed, to probe small-scale statistical behaviours of active and passive scalars advected by the same flow, it is important to have different realisations of the large-scale fluctuations due to the injection mechanisms (i.e. to the boundary conditions), otherwise the two scalar fields are trivially identical.

To reduce the effects of inhomogeneity, we measured statistical properties only in horizontal planes, within the so-called well-mixed layer, where scalar fluctuations are practically independent of the distance from the bottom wall and from the top layer.

Anisotropy is also an issue in the ABL. It is due to both buoyancy and shear. In the surface layer, the flow is characterised by the presence of streaky structures almost parallel to the horizontal direction. To cope with them (even if their effect is strongly reduced in the mixed-layer), we measured scalar fluctuations along the spanwise direction and indeed obtained scalar increment probability density functions almost symmetrical. It is worth mentioning that, despite large-scale anisotropy, scalar increment statistics measured in a convective ABL recover isotropy at scales much smaller than the integral ones. Moreover, the tendency to recover isotropy in the inertial range is a genuine feature, neither due to SGS nor to finite size effects [26].

The PDFs of the temperature and passive scalar spatial increments were computed and compared. The core of these PDFs, or equivalently the low order positive moments, showed almost indistinguishable scaling properties. Indeed, temperature and tracer spectra show the same scaling behaviour.

However, when measuring the statistical behaviour of large fluctuations, belonging to the tails of the scalar increment PDFs, it was found that the passive scalar is less intermittent than the temperature field. Both scalars exhibit saturation in the statistical behaviour of large fluctuations, but the saturation scaling exponents are different. We measured $\xi_\infty = 0.6 \pm 0.2$ for the temperature field, and $\zeta_\infty = 1.2 \pm 0.2$ for the tracer one. Saturation of scaling exponents has a clean geometrical interpretation: scalar fluctuations $\delta_r\bar{\theta}$ or $\delta_r\bar{c}$, over small scales r, are dominated by quasi-singular structures where scalar differences between two nearby points jump by $O(\lambda\sigma_{\bar{\theta}})$.

Indications of temperature statistics being more intermittent than the passive scalar one, within the same flow, were also found in the Rayleigh–Bénard experiment described in [8]. Although the boundary layer atmospheric convection presents differences from thermal convection between two plates at fixed temperatures, we think that these systems have qualitative similarities. In particular, the presence of boundaries allows us to obtain a range of scales where buoyancy transfer of energy might be dominant. This happens near the walls in a Rayleigh–Bénard cell, and in proximity of the bottom surface in the convective ABL. In our numerical simulations, this statement is supported by the measurement of the Bolgiano length, which can become much smaller than the horizontal integral scale. This is likely to be the origin of the observed different behaviour of large fluctuations of temperature and concentration fields.

Progress by numerical or laboratory experiments is hampered by difficulties in obtaining 3D datasets with wide separations of scales and with sufficient statistical convergence for high-order moments.

In the direct numerical simulations of homogeneous turbulence reported in [28] and [36], a perfect control is possible on the way forcing injects scalar fluctuations; this is less trivial in experiments or in Large-eddy Simulations such as those here presented. Future research on scalar turbulence in non-homogeneous convection (with walls) should better highlight the role of plumes, their temporal and spatial stability: these points need to be solved in order to understand the observed quantitative differences among passive scalar and thermal fronts. The situation of passive and active scalar statistics in 3D *homogeneous* convection (without walls), might be well different and remains to be clarified.

Acknowledgements

Helpful discussions with Luca Biferale, Massimo Cencini, Andrea Mazzino, Anna Maria Sempreviva and Federico Toschi are gratefully acknowledged. Numerical simulations were performed at CINECA (Italy), under the grant "Progetti di SuperCalcolo 2008", project no. 935 *Large Eddy Simulation for Planetary Boundary Layer*. We acknowledge financial support from Consiglio Nazionale delle Ricerche, within the grant "Curiosity Driven Research RSTL 2007".

References

[1] B. Shraiman, E. Siggia, Scalar turbulence, Nature 405 (2000) 639.
[2] Z. Warhaft, Passive scalars in turbulent flows, Annu. Rev. Fluid Mech. 32 (2000) 203–240.
[3] G. Falkovich, K. Gawędzki, M. Vergassola, Particles and fields in fluid turbulence, Rev. Mod. Phys. 73 (2001) 913–975.
[4] R.H. Kraichnan, Anomalous scaling of a randomly advected passive scalar, Phys. Rev. Lett. 72 (1994) 1016.
[5] A. Celani, A. Lanotte, A. Mazzino, M. Vergassola, Universality and saturation of intermittency in passive scalar turbulence, Phys. Rev. Lett. 84 (2000) 2385.
[6] K. Gawędzki, A. Kupiainen, Anomalous scaling of the passive scalar, Phys. Rev. Lett. 75 (1995) 3834.
[7] A. Celani, M. Vergassola, Statistical geometry in scalar turbulence, Phys. Rev. Lett. 86 (2001) 424.
[8] S.Q. Zhou, K.-Q. Xia, Comparative experimental study of local mixing of active and passive scalars in turbulent thermal convection, Phys. Rev. E 77 (2008) 056312.
[9] A. Celani, M. Cencini, A. Mazzino, M. Vergassola, Active vs. passive scalar turbulence, Phys. Rev. Lett. 89 (2002) 234502.
[10] A. Celani, M. Cencini, A. Mazzino, M. Vergassola, Active and passive fields face to face, New J. Phys. 6 (72) (2004) 1–35.
[11] L. Biferale, I. Procaccia, Anisotropy in turbulent flows and in turbulent transport, Phys. Rep. 414 (2–3) (2005) 43–164.
[12] F. Delaudier, C. Sidi, M. Crochet, J. Vernin, direct evidences of 'sheet' in the atmospheric temperature field, J. Atmos. Sci. 51 (1994) 237.
[13] F. Pasquill, F.B. Smith, Atmospheric Diffusion, third ed., John Wiley & Sons, Ltd, New York, 1983.
[14] P. Sagaut, Large Eddy Simulation for Incompressible Flows: An Introduction, third ed., Springer, Germany, 2006.
[15] J. Deardorff, Numerical investigation of neutral and unstable planetary boundary layers, J. Atmos. Sci. 29 (1972) 91–115.
[16] J. Deardorff, Three-dimensional numerical study of the height and mean structure of a heated planetary boundary layer, Boundary-Layer Meteor. 7 (1974) 81–106.
[17] C. Moeng, A large-eddy simulation model for the study of planetary boundary-layer turbulence, J. Atmos. Sci. 41 (13) (1984) 2052–2062.
[18] P. Mason, Large-eddy simulation of the convective atmospheric boundary layer, J. Atmos. Sci. 46 (1989) 1492–1516.
[19] S. Pope, Turbulent flows, Cambridge University Press, Cambridge, UK, 2000.
[20] A.S. Monin, A.M. Yaglom, Statistical Fluid Mechanics, MIT Press, Cambridge, USA, 1975.
[21] C.H. Moeng, P.P. Sullivan, A comparison of shear and buoyancy driven boundary layer flows, J. Atmos. Sci. 51 (7) (1994) 999–1022.

[22] M. Germano, U. Piomelli, P. Moin, W. Cabot, A dynamic subgrid-scale eddy viscosity model, Phys. Fluids A 3 (7) (1991) 1760–1765.
[23] D. Lilly, A proposed modification of the Germano subgrid-scale closure method, Phys. Fluids A 4 (1992).
[24] R.B. Stull, An Introduction to Boundary Layer Meteorology, Kluwer Academic Publishers, Dordrecht, The Netherlands, 1988.
[25] M. Antonelli, A. Mazzino, U. Rizza, Statistics of temperature fluctuations in a buoyancy-dominated boundary layer flow simulated by a large eddy simulation model, J. Atmos. Sci. 60 (2003) 215–224.
[26] M. Antonelli, A. Lanotte, A. Mazzino, Anisotropy and universality of boyancy-dominated turbulent fluctuations: a large-eddy simulations study, J. Atmos. Sci. 64 (2007) 2642–2656.
[27] E.D. Siggia, High Rayleigh number convection, Annu. Rev. Fluid Mech. 26 (1994) 137.
[28] A. Celani, T. Matsumoto, A. Mazzino, M. Vergassola, Scaling and universality in turbulent convection, Phys. Rev. Lett. 88 (2002) 054503.
[29] D. Lohse, K.-Q. Xia, Small-scale properties of turbulent Rayleigh–Bénard convection, Annu. Rev. Fluid Mech. 42 (2010) 335–364.
[30] E. Calzavarini, F. Toschi, R. Tripiccione, Evidences of Bolgiano–Obukhov scaling in three-dimensional Rayleigh–Bénard convection, Phys. Rev. E 66 (2002) 016304.
[31] R. Benzi, F. Toschi, R. Tripiccione, J. Stat. Phys. 93 (3) (1998).
[32] U. Frisch, Turbulence: The Legacy of A.N. Kolmogorov, Cambridge University Press, Cambridge, UK, 1995.
[33] I. Mazzitelli, A.S. Lanotte, Scalar turbulence in convective boundary layers with different entrainment fluxes, 2011 (submitted).
[34] F. Moisy, H. Willaime, J. Andersen, P. Tabeling, Passive scalar intermittency in low temperature helium flows, Phys. Rev. Lett. 86 (2001) 4827–4830.
[35] Indeed, because of the statistical constraint of convexity for the structure function scaling exponents, the saturation exponent is positive and $\xi_\infty \geq \xi_p$ for $p \leq p_{crit}$ [32].
[36] T. Watanabe, T. Gotoh, Statistics of a passive scalar in homogeneous turbulence, New J. Phys. 6 (2004) 40.
[37] S. Zhou, K.-Q. Xia, Plume statistics in thermal turbulence: mixing of an active scalar, Phys. Rev. Lett. 89 (18) (2002) 184502.
[38] A. Celani, A. Lanotte, A. Mazzino, M. Vergassola, Fronts in passive scalar turbulence, Phys. Fluids 13 (2001) 1768.
[39] E.S.C. Ching, Y. Cohen, T. Gilbert, I. Procaccia, Active and passive fields in turbulent transport: the role of statistically preserved structures, Phys. Rev. E 67 (2003) 016304.
[40] Note that the values of the structure functions scaling exponents, and thus of the saturation exponent ξ_∞ also, change with the statistics of the advecting flow. Universality of passive scalar statistics is with respect to the large-scale forcing, for a given velocity field.